(Received 20 February 2024, Accepted 5 April 2024, Scheduled 24 April 2024)

Research on a Current Reconstruction Method of Multi-Core Cable Based on Surface Magnetic Field Measurements

Ruixi Luo*, Yuyi Qin, Yifei Zhou, Fuchao Li, and Ruihan Wang

State Grid Sichuan Power Company, Chengdu 610045, China

ABSTRACT: The measurement and decoupling of currents in multi-core power cables is a significant concern for power operators and holds immense potential for optimizing the monitoring and control of urban distribution networks. This paper aims to provide a widely applicable method for reconstructing current measurements. A YJLV22-3∗300 power cable is taken as an example, specifically focusing on the effect of steel armor on the measurement of the magnetic field generated by the current. Sample tests and field experiments are conducted to verify the spatial distribution of the magnetic flux density. Then the inverse problem of calculating current from the magnetic field is discussed. The defects of the existing methods are shown, and a new method for the inverse problem with the measured waveform of the tangential component of the magnetic flux density is proposed. The feasibility of the new method has been verified. The least-squares method is introduced to obtain the generalized inverse of the position coefficient matrix by maximum rank decomposition to extrapolate the conductor current matrix. A query method is proven to efficiently generate this matrix. Finally, the inverse problem is modeled as a stochastic search problem to compare the efficiency and stability of different algorithms, and CAM-ES performs best. The future research direction is toward developing and testing hardware measurement systems.

1. INTRODUCTION

In the context of the growing integration of artificial intelligence technology with industrial production, acquiring real-time load current data from every node in the distribution network has emerged as a key concern for power operators. The data is essential for leveraging big data analytics to optimize distribution network planning and control strategies [1, 2]. In sprawling urban distribution networks, multi-core power cables constitute a significant portion, yet only a limited number of terminal nodes are capable of current measurement. This limitation arises from the challenge of measuring and isolating current in multi-core power cables using conventional methods. The measurement of current in the power grid can be classified into two methods: invasive and noninvasive. Among them, invasive measurement methods, such as CT (current transformers) and shunt resistors, offer high accuracy, stability, and well-established technology. However, they face challenges in terms of convenience. As a result, invasive measurement is predominantly utilized in high-voltage measurement scenarios, such as substations. On the other hand, noninvasive measurement methods, including Rogowski coils and optical sensors, do not require direct contact with the circuit being measured. These methods do not disrupt the measured circuit and are more suitable for application in low-voltage distribution networks. Nevertheless, the main noninvasive measurement methods face difficulties in achieving magnetic field decoupling and independent measurement of conductor current because the external space flux is a composite flux generated by the multi-phase current. To address this issue, a viable solution involves utilizing a magnetic sensor array to measure the magnetic field at the outer surface space of the cable and then inverting and reconstructing the current and position information in the measured conductor [3].

In recent years, the advancement of magnetic field sensor technology has led to an increasing number of studies exploring the application of sensors (such as Hall, tunnel magneto-resistive, and giant magneto-resistive sensors) for current measurement [4]. These sensors offer a hardware foundation for non-intrusive current measurement in cables. Various computational tools have been employed for reconstructing cable currents, including analytical methods, finite element method (FEM), and stochastic optimization algorithms. Geng et al. [5] present an analytical-only approach for reconstructing currents and identifying conductor locations within a closed enclosure. Building upon this idea, Kadechkar et al. [6] extend the approach to substation conductors, while Zhang et al. [7] consider three-dimensional reconstructions, accounting for conductor tilting. Further developments on the derivation and experimentation for the three-dimensional case are discussed in [8]. To enhance the flexibility of the algorithms, particularly for multi-core cables where the positions of each phase's conductors may not be known, several articles have introduced stochastic optimization algorithms based on the analytical method. Examples include particle swarm algorithm [9] and differential evolutionary algorithm [10]. However, it should be noted that the analytical method involves complex derivations and incorporates many approximation conditions. The use of FEM for current reconstruction has also been investigated [11, 12]. These studies utilize FEM and integrate stochastic optimization algorithms. However, the explicit deduction of solutions for the inversion

* Corresponding author: Ruixi Luo (lrx2947@163.com).

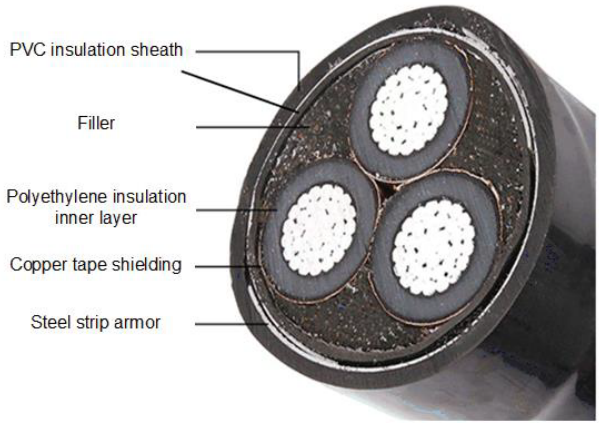

FIGURE 1. Geometric structure of YJLV22-3∗300 cable.

Name	Inner radius (mm)	Outer radius (mm)
PVC insulation sheath (outer)	39	42.5
PVC insulation sheath (inner)	37.1	38.6
Filler	-	37.1
Polyethylene insulation inner layer	11	16
Copper tape shielding layer	16	16.04
Steel strip armor	38.6	39
Conductor	-	11

TABLE 1. Geometric parameters of the YJLV22-3∗300 cable.

of phase currents from the measured magnetic field is not provided in the text. Additionally, the linearity assumption between the magnetic field and current has not been verified in the presence of steel tape armor [13]. Regarding the generalized inverse approach, Canova et al. [14] present a process derivation. However, it is not entirely applicable to the inverse problem addressed in this paper. Thus, there are still numerous questions surrounding the algorithms for solving the inverse problem of reconstructing current from the surface magnetic field of multi-core cables that require further exploration.

This paper delves into the comprehensive study of the forward and inverse problems associated with power cable current and magnetic field. The forward problem section begins by selecting a commonly used cable type and summarizing its structure, geometric dimensions, and electromagnetic parameters. Of particular interest is the effect of the magnetic steel tape armor's permeability on the cable surface's magnetic field. By conducting sample detection, an accurate permeability curve for the steel armor is obtained. FEM is employed to verify the relationship between the shielding effect resulting from the magnetization current of the steel tape armor and its permeability. Experimental procedures are conducted to validate the spatial distribution of magnetic induction intensity. Subsequently, the inverse problem section analyzes the limitations of existing methods for solving inverse problems and proposes a novel approach that utilizes the measured waveform of the tangential component of magnetic flux density for deriving the inverse problem. The feasibility of this new approach is confirmed through simulation and experimentation, establishing the proportional relationship between the tangential component of magnetic induction intensity and the current in the conductor. The principle of the least squares method is then introduced, and the generalized inverse of the position coefficient matrix is obtained through maximum rank decomposition to invert the conductor current matrix. To solve real-coded constrained single-objective optimization problems, the CMA-ES algorithm is demonstrated as an efficient and rapid solution after modeling the random search problem. Comparisons conducted among fourteen algorithms substantiate the efficacy and speed of the CMA-ES algorithm. Furthermore, the algorithm's accuracy and immunity are also confirmed.

2. FORWARD PROBLEM: CALCULATE THE MAGNETIC FIELD FROM CURRENT

According to the number of conductors, power cables can be divided into single-core and multi-core types. In urban distribution networks with voltages up to 35 kV, multi-core cables are mainly used, and a large majority of them are equipped with magnetic steel tape armor. A YJLV22-3∗300 cable model was selected as the subject of analysis and measurement. This model is widely used in China and is considered representative. The structure of the cable model is shown in Fig. 1. The structure consists of a conductor, polyethylene insulation inner layer, copper tape shielding layer, filler, polyvinyl chloride (PVC) insulation sheath, and steel strip armor from inside to outside, with the geometric dimensions and electromagnetic parameters of each component shown in Table 1 and Table 2, respectively. It should be noted that there are discrepancies in the raw material formulation and structural design by different manufacturers, so the geometric dimensions were attained by field measurements.

Due to variations in material and manufacturing processes, the magnetic permeability of the steel tape armor presented in Table 2 is not constant, but rather ranges from hundreds to thousands of values [15, 16]. According to the Biot-Savart law

$$d\vec{B} = \frac{\mu_0}{4\pi} \frac{Id\vec{l} \times \vec{r}}{r^2} \tag{1}$$

where μ_0 is the vacuum permeability. Under the condition of a quasi-static field, the flux density and current change instantaneously. Considering that the predominance of the cable current's power frequency component is a 50 Hz sine wave, the primary mechanism through which the magnetic medium affects the magnetic field distribution is the "shunt shielding mechanism" [17]. To explain the mechanism, firstly, the tangential component of the magnetic field intensity must be continuous, and the normal component of the magnetic flux density must

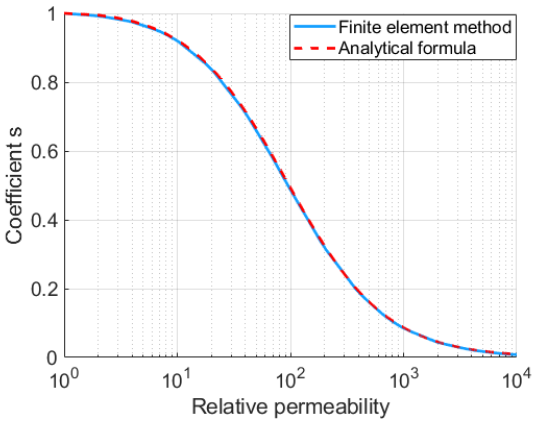

FIGURE 2. Attenuation coefficient s and relative permeability curve.

Name	μ_r	ε_r	σ_s (s/m)
PVC insulation sheath	1.0	2.7	0.0
Filler	1.0	1.0	0.0
Polyethylene insulation inner layer	1.0	2.25	0.0
Copper tape shielding layer	1.0	1.0	5.8×10^7
Steel strip armor	-	1.0	1.1×10^7
Conductor	1.0	1.0	3.8×10^7

TABLE 2. Electromagnetic parameters of YJLV22-3∗300 cable.

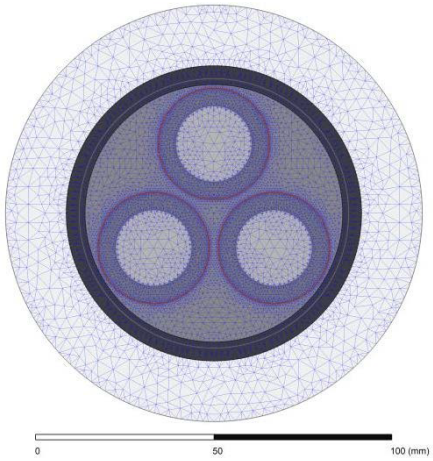

FIGURE 3. FEM model and mesh.

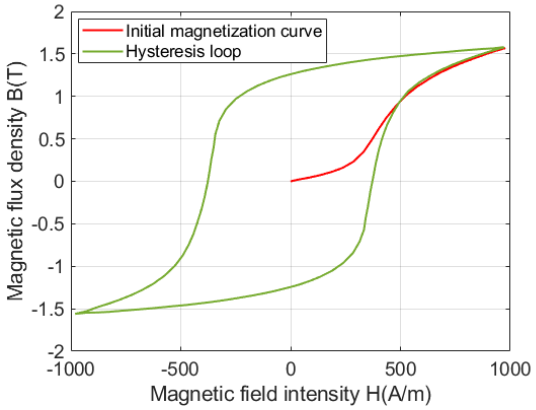

FIGURE 4. Magnetization curves of steel tape armor.

be continuous at the interface, i.e.,

$$\vec{n} \times \left(\vec{H}_1 - \vec{H}_2\right) = 0 \tag{2}$$

$$\vec{n} \cdot \left(\vec{B}_1 - \vec{B}_2\right) = 0 \tag{3}$$

Due to the difference in magnetic permeability within the ferromagnetic material and in the air, the field and flux density then must change direction abruptly as they cross the interface. As a result, the magnetic flux produced by the source is concentrated within the shielding material. In some specific source configurations and magnetic field shielding structures, the ratio of the magnetic flux density at any point outside the shielding region before and after adding the shielding is constant. For example, in a long cylindrical shielding with an outer diameter of b and an inner diameter of a, when a dipole source is placed inside the shielding, coefficient s is [17]

$$s = \frac{4\mu_r}{\left(\mu_r + 1\right)^2 - \dfrac{a^2}{b^2}\left(\mu_r - 1\right)^2} \tag{4}$$

For a three-phase cable with ferromagnetic armor, it is difficult to derive such an analytical equation about coefficient s, so an FEM-based method is used. The relationship between the coefficient s and permeability is determined by FEM and (4), as shown in Fig. 2, proving the correctness of the FEM calculations. The solid line illustrates the results obtained from the FEM calculation, while the dashed line represents the results obtained using (4). It is evident that the FEM accurately captures the impact of the magnetic medium on the distribution of magnetic fields.

To assess the impact of the steel armor permeability on the actual magnetic field distribution, the numerical solution provided by FEM will be utilized, considering the magnetic shielding and the complexity of the cable structure. The cable is assumed to be long and straight, without any bends, and the current in each phase conductor solely flows along the cable's extension direction, allowing it to be represented as a two-dimensional model. The established finite element model is shown in Fig. 3.

The influence of radial displacement current (leakage current of the cable) is ignored in the calculation. Meanwhile,

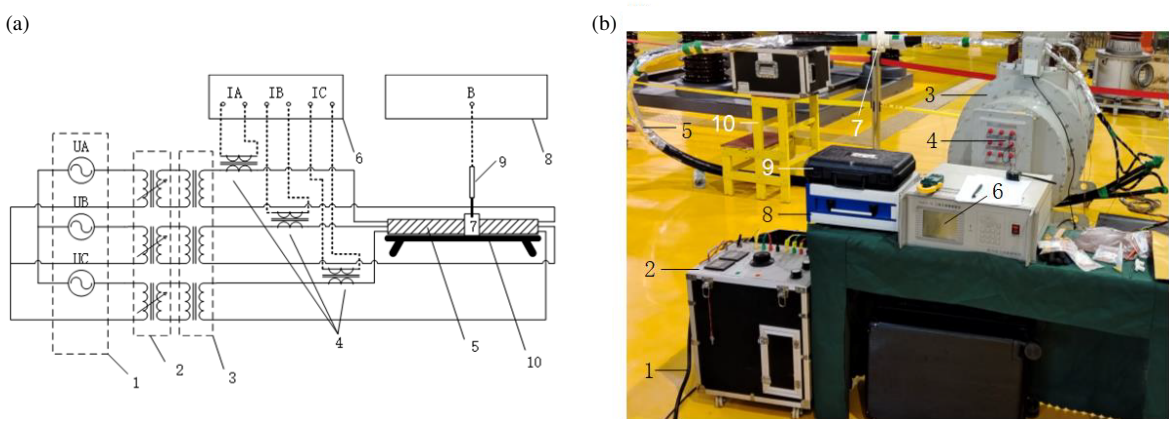

FIGURE 5. The experimental platform, (a) schematic diagram, (b) on-site setup.

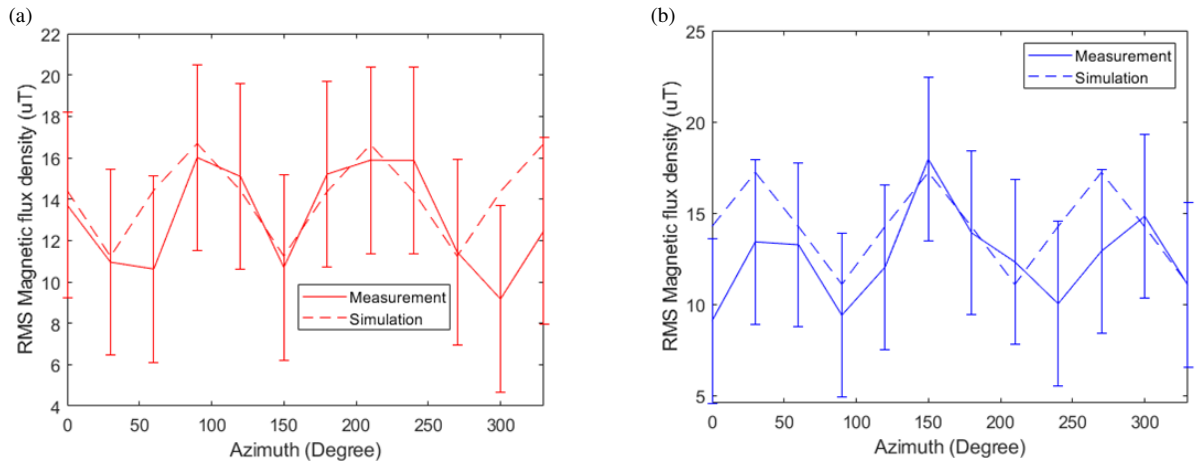

FIGURE 6. Spatial distribution of the RMS of the magnetic flux density 15 mm from the cable surface, (a) radial component, (b) tangential component.

the B-H magnetization curve of the steel armor under test is obtained through sample detection, and the permeability value corresponding to the current can be further obtained as a constant. The curve is shown in Fig. 4.

An experiment was carried out to verify the correctness of the simulation. The schematic diagram of the experimental platform and the field construction are shown in Fig. 5. This experimental platform consists of the following parts: 1. Three-phase power supply; 2. Voltage regulator; 3. Current Booster; 4. Standard current transformer; 5. Multi-core cable; 6. Current comparator; 7. Adjustable fixture for magnetic field probes; 8. Magnetometer; 9. Magnetic field probe; 10. Multi-core cable supporting tool. The rest of the platform on the conductor portion is wrapped with magnetic shielding material to minimize the effect of errors.

The test evaluation uses a high-precision triaxial magnetic field probe to achieve accurate magnetic field measurement, and the error does not exceed 4.5 μT in the range of 3 mT.

By adjusting the fixture, measurement points were placed at an interval of 30° azimuthal angle and 15 mm from the cable surface to obtain the spatial distribution of the RMS (root mean square) of the tangential component of the magnetic flux density $\mathbf{B}_\tau$ as well as the radial component $\mathbf{B}_r$, and the comparison with the simulation results of the relative measurement points is shown in Fig. 6, with the background magnetic field measured in the field being 0.94 μT for $\mathbf{B}_\tau$ and 1.28 μT for $\mathbf{B}_r$.

The meaning of the data obtained from the test needs to be clarified here. Tangential and radial directions are interpreted as follows: for a point on a circle, its line to the center of the circle is the radius of the circle; the direction parallel to this radius and pointing to the center of the circle is radial, and the counterclockwise direction perpendicular to this radius is tangential. The RMS is the arithmetic square root of the mean of the squares of a set of data.

Figure 6 shows that the range of the values of the magnetic flux density is similar, and all of them are in line with the peak/valley reciprocal correspondence between the $\mathbf{B}_\tau$ curve and the $\mathbf{B}_r$ curve. According to [18], the unbalanced spatial distribution of phase conductors may lead to changes in the spatial distribution of the magnetic flux density around the cable, so the experimental results are slightly different from those in the simulation. At this point, all aspects of the forward problem of the current generation in the cable phase conductors generating a magnetic field on the cable surface have been clarified or ver-

ified, and the study of the inverse problem will be carried out next.

3. INVERSE PROBLEM: CALCULATE CURRENT FROM THE MAGNETIC FIELD

Reconstructing the currents in the conductors of each phase of the cable based on the magnetic field measured outside the cable is the primary objective in solving the inverse problem. In this paper, a method is proposed to minimize the difference between measurement and calculation of the tangential component of magnetic flux density, namely

$$\min \left\| \mathbf{B}_{\tau}^{mea} - \mathbf{B}_{\tau} \right\|_2 \tag{5}$$

where $\mathbf{B}_{\tau}$ is calculated using

$$\mathbf{B}_{\tau} = \mathbf{PI} \tag{6}$$

The position coefficient matrix $\mathbf{P}$ is difficult to obtain in the presence of steel armor, and a query method is proposed to solve the problem. Next, the concept of generalized inverse matrices is introduced to solve Equation (6). Finally, the conductor position is generated by the stochastic optimization algorithm; the optimal conductor position is obtained through iterative calculation; and the current reconstruction is completed at the same time. The flowchart of the above algorithm is shown in Fig. 7.

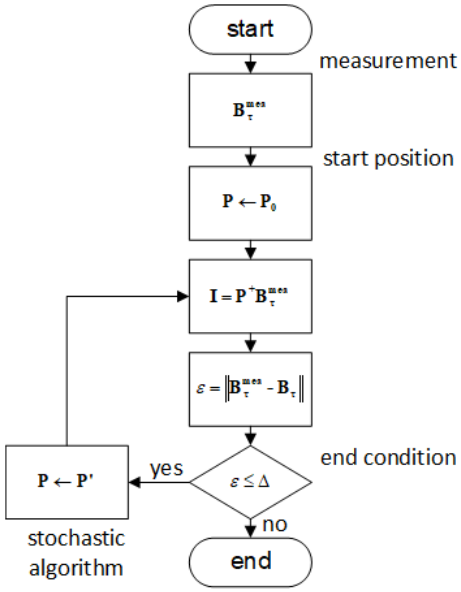

FIGURE 7. The flowchart of the algorithm.

3.1. Variable to be Solved

The selection of an appropriate variable to be solved is crucial as it directly impacts the problem modeling and the validity of the solution. In other words, which parameter of magnetic field measurement can be used to reconstruct the current? Existing literature primarily employs the magnitude of the magnetic flux density [5–10]. However, the magnitude of the magnetic flux density used represents the vector sum of its tangential and radial components. In practical sensors, these components are measured separately, and the two sensitive axes are not strictly vertical [22]. The existing calibration method for magnetic field sensors is used to calibrate 2-axis sensors [23], but it defaults to the two sensing axes perpendicular to each other. This method can also be applied to single-axis sensors.

This paper uses the measured waveform of the tangential component of the magnetic flux density, i.e., a series of data with equal time intervals (the reciprocal of the sampling rate). Consequently, with the known linear coefficient, the current waveform can be inverted theoretically with measurement data to obtain the parameters such as amplitude, phase, and additional pertinent information.

The radial component of the magnetic flux density is not considered the main variable to be solved. If the center of one conductor is located closer to the line connecting the measurement point with the geometric center of the cable cross-section, the linearity coefficient brought by this conductor is nearly 0, which can be smaller than the resolution of the sensor.

3.2. Equation Establishment

This approach operates under the condition that the instantaneous value of the tangential component $\mathbf{B}_{\tau}$ of the magnetic flux density at point p, external to the cable, can be expressed as a linear combination of the currents flowing within the three-phase conductors enclosed by the cable, namely

$$B_{\tau}(p,t) = p_A(t) I_A(t) + p_B(t) I_B(t) + p_C(t) I_C(t) \tag{7}$$

where $p_A(t)$, $p_B(t)$, and $p_C(t)$ are the linear coefficients of each phase conductor, whose exact magnitude is related to the position of each phase conductor and specific moment due to the hysteresis effect of ferromagnetic armor. But in the actual calculation, the linear coefficients are treated as time-invariant constants, because the typical load current corresponds exactly to the linear region of the B-H curve. This will, of course, cause calculation errors, which will be explained and evaluated in subsequent work. Therefore, this equation can be regarded as a ternary equation, with the unknowns in the equation being the instantaneous values of the three-phase currents.

It should be noted that the magnitude of the linear coefficients in (6) is related to the position of the conductor in each phase, where the position refers to the coordinate position of the conductor concerning each measurement point, so that there are several ternary equations with different linear coefficients for several measurement points (at a given moment), and writing these sets of equations for each moment in matrix form, we have

$$\begin{bmatrix} B_{\tau 1}(t) \\ B_{\tau 2}(t) \\ B_{\tau 3}(t) \\ \cdots \end{bmatrix} = \begin{bmatrix} p_{A1} & p_{B1} & p_{C1} \\ p_{A2} & p_{B2} & p_{C2} \\ p_{A3} & p_{B3} & p_{C3} \\ \cdots & \cdots & \cdots \end{bmatrix} \cdot \begin{bmatrix} I_A(t) \\ I_B(t) \\ I_C(t) \end{bmatrix} \tag{8}$$

This can be further simplified as (6).

3.3. Position Coefficient Matrix Generation

Considering the effects of the skin effect and magnetic shielding effect, FEM emerges as the most suitable method to obtain the matrix P from a set of conductor center positions given by

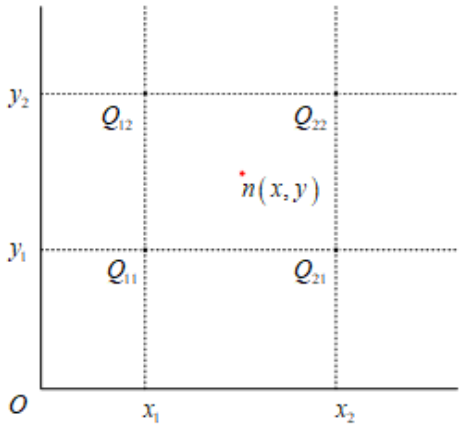

FIGURE 8. A schematic diagram of linear interpolation.

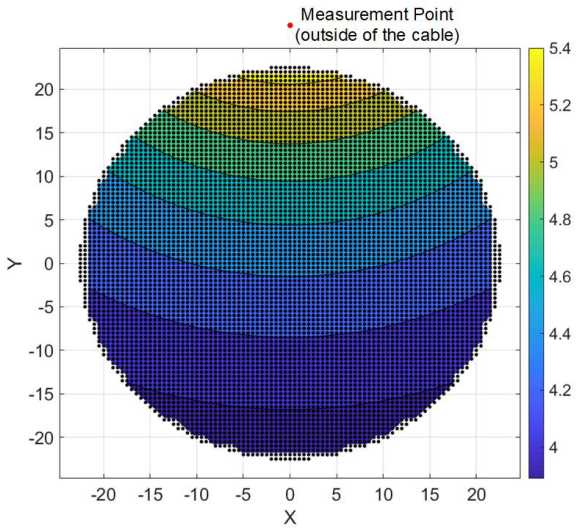

FIGURE 9. Distribution of linear coefficients.

a stochastic algorithm. Since the stochastic algorithm will attempt a large number of conductor positions, and each conductor position change will lead to finite element mesh division and linear equation solving, the time cost of multiple FEM executions is unacceptable. To solve this problem, a query method is introduced to reduce the complexity and computing power consumption of stochastic algorithm processes.

The query method means that before starting the random search algorithm, the linear coefficients of some positions are obtained in ANSYS, and then the linear coefficients of all positions are generated by linear interpolation. In this way, a database is established, and the database can be queried for the corresponding linear coefficients for a set of conductor center positions given by the random search.

The matrix of linear coefficients corresponding to different positions in the feasible domain inside the cable is generated at 0.5 mm intervals. In the process of generating the matrix, because the upper and lower semicircles inside the cable are equivalent for each sensor, the amount of computation can be halved. The interpolated contour distribution obtained here is shown in Fig. 9. The querying of the database is carried out by a structure-function $f(x, y)$. For a conductor position $m(x, y)$, its corresponding linear coefficients are

$$p_m = f(x, y) \tag{9}$$

where

$$\begin{aligned} f(x,y) \;=\; & \frac{f(Q_{11})}{(x_2-x_1)(y_2-y_1)}(x_2-x)(y_2-y) \\ & + \frac{f(Q_{21})}{(x_2-x_1)(y_2-y_1)}(x-x_1)(y_2-y) \\ & + \frac{f(Q_{12})}{(x_2-x_1)(y_2-y_1)}(x_2-x)(y-y_1) \\ & + \frac{f(Q_{22})}{(x_2-x_1)(y_2-y_1)}(x-x_1)(y-y_1) \end{aligned} \tag{10}$$

The points and coordinate values in (10) are shown in Fig. 8. The positions generated at equal intervals divide the cable cross-section plane into squares. The vertex of each square is marked as Q_{11}, Q_{12}, Q_{21}, and Q_{22}, respectively. The linear coefficient corresponding to any point in the square is obtained by linear interpolation by (10). In this way, the linear coefficient of any point in the feasible domain can be obtained.

The aforementioned method enables the acquisition of a database specific to a single measurement point. To extend the application of this method to derive linear coefficients for another measurement point located at the same distance from the center of the cable but at a different azimuthal angle, a two-step process needs to be engaged. Initially, the coordinates of the initial measurement point are dot multiplied by the rotation matrix, as shown in (11). Subsequently, these transformed coordinates are substituted into (9), computing the corresponding coefficients for another measurement point. Furthermore, it is crucial to note that the angle in the rotation matrix is the opposite of the difference in azimuths of the actual two measurement points, i.e.,

$$\begin{aligned} & p_n = f(x', y') \\ & s.t. \begin{cases} \begin{bmatrix} x' \\ y' \end{bmatrix} = \begin{bmatrix} \cos\theta & \sin\theta \\ -\sin\theta & \cos\theta \end{bmatrix} \begin{bmatrix} x \\ y \end{bmatrix} \\ \angle mOn = \theta \\ \sqrt{x^2+y^2} = \sqrt{x'^2+y'^2} \end{cases} \end{aligned} \tag{11}$$

where O is the center of the cable, and θ is the azimuth difference between m and n and positive clockwise.

3.4. Equation Solving

When the position coefficient matrix **P** is uniquely determined based on the three-phase conductor center positions, for a set of positions given by the random search algorithm, there is a unique corresponding position coefficient matrix **P**. At

this time, there exists a unique conductor current matrix that makes (9) hold. To obtain this conductor current matrix, the Moore-Penrose generalized inverse is used, and the first step is to perform a maximal rank decomposition on $\mathbf{P}$ of size $m \times n$ and rank $\mathbf{P} = r$, which is

$$\mathbf{P} = \mathbf{CD} \tag{12}$$

where $\mathbf{C}$ is an $m \times r$ matrix, $\mathbf{D}$ an $r \times n$ matrix, and rank $\mathbf{C} =$ rank$\mathbf{D} = r$. Thus, the generalized inverse of $\mathbf{P}$ corresponding to (9) is [19],

$$\mathbf{P}^{+} = \mathbf{D}^{\mathbf{H}} \left(\mathbf{D}\mathbf{D}^{\mathbf{H}}\right)^{-1} \left(\mathbf{C}^{\mathbf{H}}\mathbf{C}\right)^{-1} \mathbf{C}^{\mathbf{H}} \tag{13}$$

where H denotes the conjugate transpose, and -1 denotes the inverse matrix. For the $\mathbf{P}$ matrix in this problem, since the equation $\mathbf{PI} = 0$ has only zero solutions, $\mathbf{P}$ is column-full rank, so the maximum rank decomposition of $\mathbf{P}$ becomes

$$\mathbf{P} = \mathbf{PE} \tag{14}$$

where $\mathbf{E}$ is the identity matrix. Since $\mathbf{P}$ is a real matrix whose conjugate transpose is equal to its transpose, the generalized inverse of $\mathbf{P}$ is reduced to

$$\mathbf{P}^{+} = \left(\mathbf{P}^{\mathbf{T}}\mathbf{P}\right)^{-1} \mathbf{P}^{\mathbf{T}} \tag{15}$$

So, the formula for the inverse conductor current matrix can be obtained

$$\mathbf{I} = \mathbf{P}^{+}\mathbf{B}_{\tau}^{\mathbf{mea}} \tag{16}$$

Regarding $\mathbf{PI} = 0$, why there are only zero solutions, i.e., the columns of the $\mathbf{P}$ matrix are linearly independent, it can be proved as follows: when the position of the center of each conductor lies on the same linear coefficient contour for different measurement points, there is a non-zero solution; therefore, if there is only one measurement point, the columns of the $\mathbf{P}$ matrix are linearly related; and if there are two measurement points with azimuth angles relatively close to each other, the contour lines may have an intersection point, and the columns of the $\mathbf{P}$ matrix are linearly related; if there is a large difference between the azimuths of two measurement points, or there are more than or equal to three measurement points, the columns of the $\mathbf{P}$ matrix are linearly uncorrelated. If $\mathbf{P}$ is not a column-full rank matrix, its maximum rank decomposition form is not unique, and the uniqueness of the solution (conductor position) of the inverse problem is not satisfied at this point.

3.5. Stochastic Algorithm

For an optimization problem based on a stochastic search strategy, its fitness function needs to be defined, and the fitness function, i.e., the objective function, can be directly defined according to (11) as

$$F = \left\|\mathbf{B}_{\tau}^{\mathbf{mea}} - \mathbf{B}_{\tau}\right\|_2 \tag{17}$$

The value of three-phase current when it takes the minimum value is the optimal solution of current in the system of equations. Let the three-phase conductor center position be $(x_A, y_A)(x_B, y_B)(x_C, y_C)$. Then the optimization problem satisfies the inequality constraints of the fitness function:

$$\begin{aligned}
&x_A^2 + y_A^2 \le (R_{in} - R_p)^2 \\
&x_B^2 + y_B^2 \le (R_{in} - R_p)^2 \\
&x_C^2 + y_C^2 \le (R_{in} - R_p)^2 \\
&(x_A - x_B)^2 + (y_A - y_B)^2 \ge (2R_p)^2 \\
&(x_A - x_C)^2 + (y_A - y_C)^2 \ge (2R_p)^2 \\
&(x_C - x_B)^2 + (y_C - y_B)^2 \ge (2R_p)^2
\end{aligned} \tag{18}$$

where R_{in} is the inner radius of the PVC insulation sheath (inner), and R_p is the radius of each conductor, namely the outer radius of the copper tape shielding layer. These conditions are such that the phase conductors cannot exceed the steel armor boundary and do not overlap each other.

In this paper, we are going to solve a real number coded single objective optimization problem with constraints, and we compare fourteen algorithms that are commonly used to solve this type of problem [20]: ABC (Artificial Bee Colony), CMA-ES (Covariance Matrix Adaptation Evolution Strategy), CSO (Competitive Swarm Optimization), DE (Differential Evolution), FEP (Free Energy Perturbation), FROFI (Feasibility Rule with the incorporation of Objective Function Information), GA (Genetic Algorithm), GPSO (Gradient-based Particle Swarm Optimization), IMODE (Improved Multi-operator Differential Evolution), OFA (Optimal Foraging Algorithm), PSO (Particle Swarm Optimization), SA (Simulated Annealing), SHADE (Success-history based Adaptive Differential Evolution), and SQP (Sequential Quadratic Programming). Their performances are compared on the same problem, which is the one discussed in this paper of magnetic field inversion currents, where the positions of the three-phase conductors are set to be symmetrical, with one phase (20, 0), and the three-phase currents are also set to be balanced, with one phase having a magnitude of 100 A. For each algorithm, the population size is set to 100, and the maximum number of evaluations is 10000 (100 generations). Among them, the algorithms with fitness less than 2 after 100 generations are set as candidate algorithms: CMAES, GA, and IMODE. i.e., covariance matrix adaptive evolutionary strategies, genetic algorithms, and improved multi-operator differential evolution.

4. ALGORITHM COMPARISON AND PERFORMANCE TESTING

To compare and test the performance of the candidate algorithms, the following three aspects need to be examined: generalization, anti-interference capability, and accuracy.

For generalization, the test method is to set an initial set of parameters, use it as the base set, and randomly generate multiple sets of parameters within a certain range. Take the parameters given in the previous section as the base point. The distance between the center of the conductors and the origin varies within ± 2 mm, and the azimuth angle of them varies within $\pm 10°$. The

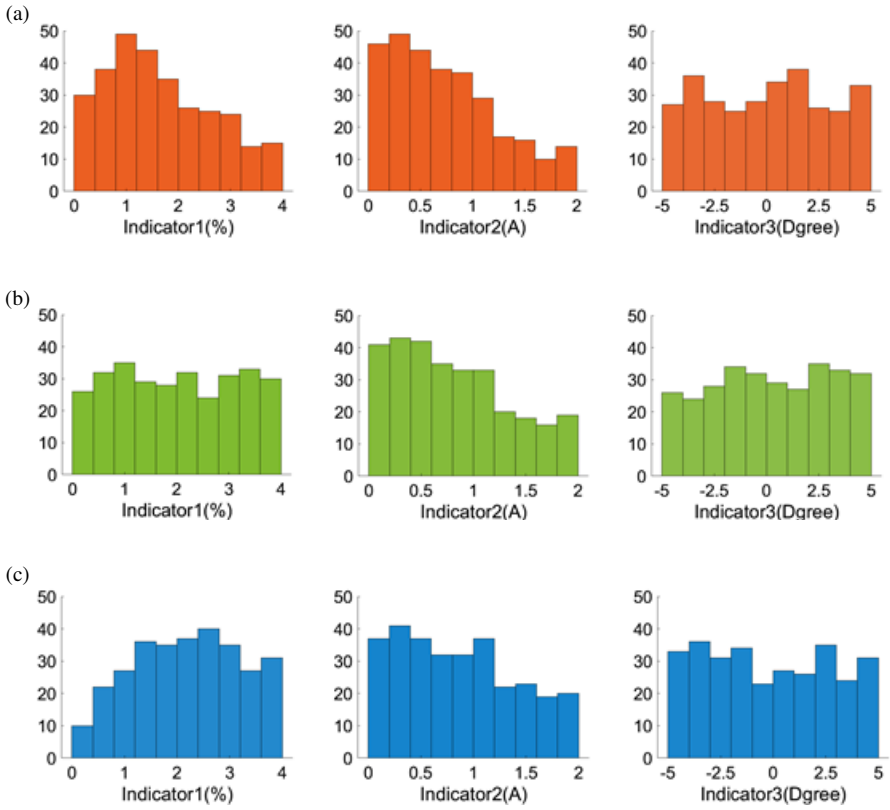

FIGURE 10. Test results of three candidate algorithms, (a) CAM-ES, (b) GA, (c) IMODE.

amplitude of the current in the conductor varies in the range of ± 10 A, and the phase of the current varies in the range of 10°.

For anti-interference capability, the test method is to introduce a random level of Gaussian noise within a range (0–2 A) in the measured magnetic field data.

For accuracy, the test method is to check the following three indicators: 1. the average relative error of the RMS of the reconstructed current waveform; 2. the average of the standard deviation of the difference between the reconstructed and actual current waveforms; 3. the angular difference between the reconstructed and actual current waveforms (fitting the data with a sine function).

$$indicator1 = \left| \frac{I_{real} - I}{I_{real}} \right| \text{(rms)} \tag{19}$$

$$indicator2 = std\left(\mathbf{I}_{real} - \mathbf{I}\right) \tag{20}$$

$$indicator3 = \angle \dot{\mathbf{I}}_{real} - \angle \dot{\mathbf{I}} \tag{21}$$

A total of 100 test samples (300 phase conductors' data in total) were randomly generated in each range described in the generalization and anti-interference capacity test methods, and the effects of the three candidate algorithms were compared in three indicators of accuracy as shown in Fig. 10. By comparison, the CAM-ES algorithm has the best performance in the three indicators. In particular, for indicator 3, which is expected to be close to 0, we take the average of the squares of each sample data as the criterion. The results of the three candidate algorithms are 8.19, 8.31, and 8.60, respectively.

The core idea of CMA-ES [21] is to deal with dependencies and scaling between variables by adjusting the covariance matrix in a normal distribution. The algorithm can be divided into the following three steps: sampling to generate a new solution; calculating the value of the objective function; and updating the distribution parameters. The core of the algorithm design is how to adjust these parameters, especially the step size parameter and covariance matrix, to achieve the best possible search effect. The adjustment of these parameters has a very important impact on the convergence rate of the algorithm.

To further test the performance of the algorithm in the absence of Gaussian noise, indicator 1, namely that the reconstruction error does not exceed 0.4% if the analytical method is used for inversion calculation, the reconstruction error will be below 0.1% when there is no ferromagnetic armor.

5. CONCLUSION

Through theoretical analysis, simulation calculation, and experimental evaluation, the analysis of the magnetic field and the current reconstruction method of multi-core power cables were studied.

The effect of the armor was evaluated, and it was concluded that the reduction in the magnetic flux density amplitude was over 80% when the relative permeability of the armor was 400.

Given the shortcomings of the existing reconstruction methods in engineering applications, the construction of the inverse

problem equation is optimized, which can reduce the error rate and save reconstruction time.

According to the performance requirements of the power cable measurement scenario, a variety of stochastic algorithms were evaluated, and the conclusion was that CMA-ES performed the best in the listed algorithms.

The reconstruction error can be controlled within 0.4% when there is no Gaussian noise in the measurement data, and the reconstruction time should not exceed 3 minutes.

In the future, a hardware measurement system will be further developed to verify the current reconstruction method proposed in this paper.

ACKNOWLEDGEMENT

This work was supported in part by the State Grid Sichuan Power Company under Grant 521997230018.

REFERENCES

[1] Li, J., *et al.*, "Real-time calculation on three-phase line loss of power distribution network based on characteristic measurement," *Guangdong Electric Power*, Vol. 30, No. 2, 81–86, 2017.

[2] Memala, W. A., C. Bhuvaneswari, S. C. Mana, M. P. Selvan, M. Maniraj, and S. Kishore, "An approach to remote condition monitoring of electrical machines based on IOT," *Journal of Physics: Conference Series*, Vol. 1770, No. 1, 012023, 2021.

[3] Ayambire, P. N. and Q. Huang, "Current source reconstruction with independent component analysis in sensor array measurement of multi-conductor current," *Journal of Electrical & Electronic Systems*, Vol. 7, No. 3, 1000264, 2018.

[4] Ziegler, S., R. C. Woodward, H. H.-C. Iu, and L. J. Borle, "Current sensing techniques: A review," *IEEE Sensors Journal*, Vol. 9, No. 4, 354–376, 2009.

[5] Geng, G., J. Wang, K.-L. Chen, and W. Xu, "Contactless current measurement for enclosed multiconductor systems based on sensor array," *IEEE Transactions on Instrumentation and Measurement*, Vol. 66, No. 10, 2627–2637, 2017.

[6] Kadechkar, A., J.-R. Riba, M. Moreno-Eguilaz, and J. Sanllehi, "Real-time wireless, contactless, and coreless monitoring of the current distribution in substation conductors for fault diagnosis," *IEEE Sensors Journal*, Vol. 19, No. 5, 1693–1700, 2019.

[7] Zhang, H., F. Li, H. Guo, Z. Yang, and N. Yu, "Current measurement with 3-D coreless TMR sensor array for inclined conductor," *IEEE Sensors Journal*, Vol. 19, No. 16, 6684–6690, 2019.

[8] Liu, X., W. He, and Z. Xu, "Non-contact current measurement method for multiconductor systems based on tunnel magnetoresistance sensor array," in *2022 IEEE International Conference on Sensing, Diagnostics, Prognostics, and Control (SDPC)*, 214–218, IEEE, 2022.

[9] Liu, Z., P. Li, C. Xu, J. Zhao, M. Xin, and B. Tian, "Non-contact current measurement method for multi-conductor in digital twin based on magnetoresistance sensors and PSO," in *2021 4th International Conference on Energy, Electrical and Power Engineering (CEEPE)*, 54–58, IEEE, 2021.

[10] Wang, H., *et al.*, "Phase current measurement method of three-core cable based on surface magnetic field inversion," *Proceedings of the CSEE*, 1–13, 2023.

[11] Sun, X., C. K. Poon, G. Chan, C. L. Sum, W. K. Lee, L. Jiang, and P. W. T. Pong, "Operation-state monitoring and energization-status identification for underground power cables by magnetic field sensing," *IEEE Sensors Journal*, Vol. 13, No. 11, 4527–4533, 2013.

[12] Zhu, K., W. Han, W. K. Lee, and P. W. T. Pong, "On-site non-invasive current monitoring of multi-core underground power cables with a magnetic-field sensing platform at a substation," *IEEE Sensors Journal*, Vol. 17, No. 6, 1837–1848, 2017.

[13] Park, M., S. Byun, W. Kim, J. Lee, K. Choi, and H. Lee, "Non-contact measurement of current distribution in parallel conductors by using Hall sensors," *IEEE Transactions on Applied Superconductivity*, Vol. 18, No. 2, 1135–1138, 2008.

[14] Canova, A., F. Freschi, M. Repetto, and M. Tartaglia, "Identification of an equivalent-source system for magnetic stray field evaluation," *IEEE Transactions on Power Delivery*, Vol. 24, No. 3, 1352–1358, 2009.

[15] Feng, H., L. Wang, and G. Li, "Study on the effect of C, N, S content on the permeability of non-oriented electrical steel," *Journal of Anhui Metallurgical Science and Technology Vocational College*, Vol. 27, No. 2, 4–5, 2017.

[16] Ke, S., H. Zhang, and Z. Ni, *Quick Reference Manual of Magnetic Curves of Commonly Used Steels*, China Machine Press, 2003.

[17] Hoburg, J. F., "Principles of quasistatic magnetic shielding with cylindrical and spherical shields," *IEEE Transactions on Electromagnetic Compatibility*, Vol. 37, No. 4, 574–579, 1995.

[18] Zhu, K., W. K. Lee, and P. W. T. Pong, "Energization-status identification of three-phase three-core shielded distribution power cables based on non-destructive magnetic field sensing," *IEEE Sensors Journal*, Vol. 17, No. 22, 7405–7417, 2017.

[19] Chen, G., *Matrix Theory and Applications*, 199–207, Higher Education Press, 1990.

[20] Tian, Y., R. Cheng, X. Zhang, and Y. Jin, "PlatEMO: A MATLAB platform for evolutionary multi-objective optimization [educational forum]," *IEEE Computational Intelligence Magazine*, Vol. 12, No. 4, 73–87, 2017.

[21] Hansen, N., "The CMA evolution strategy: A tutorial," *Arxiv Preprint Arxiv:1604.00772*, 2016.

[22] Honeywell, "3-axis magnetic sensor hybrid HMC2003," Available: https://physics.ucsd.edu/neurophysics/Manuals/-Honeywell/HMC_2003.pdf, 2016.

[23] Liu, X., "Research on the construction of non-invasive load measurement system and load disaggregation method," Ph.D. dissertation, Dept. Elect. Cn., Chongqing Univ., Chongqing, China, 2022.